

Review

An Overview of Temperature Issues in Microwave-Assisted Pyrolysis

Mattia Bartoli ¹, Marco Frediani ², Cedric Briens ³, Franco Berruti ^{3,*} and Luca Rosi ^{2,*}

¹ Department of Applied Science and Technology, Polytechnic of Turin, C.so Duca degli Abruzzi 24, 10129 Turin, Italy; mattia.bartoli@polito.it

² Department of Chemistry “Ugo Schiff”, University of Florence, Via della Lastruccia, 3-13, 50019 Sesto Fiorentino, Italy; Marco.frediani@unifi.it

³ Institute for Chemicals and Fuels from Alternative Resources (ICFAR), Department of Chemical and Biochemical Engineering, Western University, London, ON N6A 5B9, Canada; cbriens@uwo.ca

* Correspondence: fberruti@uwo.ca (F.B.); luca.rosi@unifi.it (L.R.);
Tel.: +519-661-2111 (F.B.); +39-55-4573458 (L.R.)

Received: 10 September 2019; Accepted: 25 September 2019; Published: 26 September 2019



Abstract: Microwave-assisted pyrolysis is a promising thermochemical technique to convert waste polymers and biomass into raw chemicals and fuels. However, this process involves several issues related to the interactions between materials and microwaves. Consequently, the control of temperature during microwave-assisted pyrolysis is a hard task both for measurement and uniformity during the overall pyrolytic run. In this review, we introduce some of the main theoretical aspects of the microwaves–materials interactions alongside the issues related to microwave pyrolytic processability of materials.

Keywords: microwave; pyrolysis; temperature control

1. Introduction

In the last two decades, increased societal pressure for environmental preservation and global warming mitigation has led the way to the development of new production perspectives [1,2]. Among all the innovative platforms, biorefineries and waste-to-chemicals technologies have experienced further developments [1–3]. Thermochemical processes play a relevant role in both approaches [4] with a primary emphasis on waste management [5]. Among thermochemical conversion technologies, pyrolysis is very attractive as its process conditions can be easily adjusted to maximize production of liquid fuels [6,7], chemicals [8] or carbon-based materials [9,10]. A plethora of papers [11,12] can be found in the literature all affirming that microwave-assisted pyrolysis (MAP) reduces energy consumption due to a fast volumetric heating. This is a general idea coming from a mere “ideal” situation and there is no evidence for an energy expenditure reduction yet. For example, there are no studies providing a realistic comparison between the energy consumption costs for the operation of a large-scale setup microwave oven (kW) and a gas-fired heater (including all the operational steps). Even if the MAP cost-effectiveness is still discussed [13–16], microwave thermochemical processes show a high energy efficiency when compared with traditional ones, e.g., as for organic synthesis. As a consequence, MAP has become a very powerful process to promote rapid conversion of many feedstocks to chemicals and fuels [17,18] and the use of microwave (MW)-based technologies has been exploited to develop compact and cost-effective units [16] as reported by several patents [14,15] and entrepreneurial successes [16]. However, there is a threshold power density beyond which the materials can be pyrolyzed without adding any susceptors (typically $> 10^8$ W/m³) as reported by Robinson et al. for the MAP of woody pellets [17]. Despite this, common MW equipment cannot

provide this input and MAP generally requires materials that are effective MWs absorbers. As reported by many authors, metals [18], metals–materials [19] and several carbon based materials are very effective MW absorbers [20,21]. Unfortunately, typical waste materials such as polymers and biomass are poor MW absorbers, as reported by Undri et al. [22,23] with few exceptions, such as some composites like waste tires [24] and some waste electrical and electronic equipment (WEEE) fractions [25]. Trying to address this problem, several authors reported the beneficial effect of the addition of MW absorbers to biomass [22,26,27] and plastics [28]. Undri et al. [22] clearly showed the beneficial effects of the presence of MW absorbers allowing the use of significantly lower energy density. With or without the addition of a MW absorber, MW absorption is an anisotropic process due to feedstock inhomogeneities leading to the formation of hotspots within the reactor [29].

Optimizing a MAP process is challenging [30], particularly in the case of a process focused on fuels and chemicals production [31], for which the reacting temperature must be controlled. As reported by Undri et al. [32], traditional temperature measurements in MAP are not reliable.

This paper first reviews the interactions between MWs and materials exploring the temperature critical issues during MAP.

2. Microwave (MW) Interactions with Materials: A Brief Summary

MWs range in wavelength from 10^{-3} to 1 m with an associate photon energy from 1.2 μeV to 1.2 MeV [33]. As all electromagnetic radiation, MWs are composed by two perpendicular fields, an electric (E) and a magnetic (H) one, oscillating in the frequency range of 300 MHz to 300 GHz. Several authors [34,35] reviewed the interactions between MWs (both E and H) and materials. The interactions between E or H and a material are described by the following equations, which involve the relative dielectric constant, ϵ'_r (Equation (1)), the dielectric loss, ϵ''_r (Equation (2)), the relative magnetic permeability, μ'_r (Equation (3)) and the magnetic loss, μ''_r (Equation (4)).

$$\epsilon'_r = \epsilon'/\epsilon_0 \quad (1)$$

$$\epsilon''_r = (\epsilon''/\epsilon_0) + (\sigma/2\pi f\epsilon_0) \quad (2)$$

$$\mu'_r = \mu'/\mu_0 \quad (3)$$

$$\mu''_r = (\mu''/\mu_0) + (\sigma/2\pi f\mu_0) \quad (4)$$

where ϵ' is the dielectric constant of the material, ϵ_0 is the dielectric constant of the void, ϵ'' is the dielectric loss of the material, ϵ''_0 is the dielectric loss of the void, σ is the conductivity of the material and f is the frequency of the of the MWs, μ' is the magnetic permeability of the material, μ_0 is the magnetic permeability of the void and μ'' is the magnetic loss of the material.

With non-magnetic materials, only interactions with component E of the electromagnetic field need to be considered and the parameter used to describe it is defined in Equation (5):

$$\epsilon^* = \epsilon'_r - i \epsilon''_r \quad (5)$$

where ϵ^* is the complex electric permittivity of the material.

Both ϵ'_r and ϵ''_r are influenced by several interactions, such as dipolar, interfacial, ionic and electronic ones [35]. Also, the first term of Equation (5) (ϵ'_r) is correlated to the capability of a material to store electric energy, while the second term (ϵ''_r) is responsible for the conversion of stored energy into heat. According to their electric behaviour, materials could be classified as dielectric (i.e., water [36], silica [37], alumina [38]) or conductive (i.e., salts [39], metals [40] and metal oxides [41]) materials that display different heating mechanisms under MW irradiation. Considering a perfect dielectric material, heating primarily occurs as polarization loss consisting of rapid reorientation of instant or permanent dipoles randomly distributed within the material. On the other hand, conductive materials are heated

under MWs irradiation through a different mechanism, called conduction loss, caused by the electric current generated by movements of free electrons induced by the electric field (E).

Considering materials with magnetic properties, there are many additional mechanisms that influence the heating process. The first is the hysteresis loss due the rearrangement of magnetic domains releasing magnetic energy that causes local heating. Another effect observed in magnetic materials is the Eddy currents loss caused by the formation of closed current loops that induce a current and heat dissipation [42]. The eddy currents' loss is prominent for ferromagnetic materials and it is called electron-spin loss caused by the dissipation as heat of precessional energy associated to the magnetic angular moment [43].

A rapid estimation of MW absorption can be performed using two parameters called electric and magnetic loss tangents ($\tan\delta_e$ and $\tan\delta_m$, respectively):

$$\tan\delta_e = \varepsilon''_r/\varepsilon'_r \quad (6)$$

$$\tan\delta_m = \mu''_r/\mu'_r \quad (7)$$

Commonly, non-magnetic materials are considered MWs absorbers for $\tan\delta_e$ values up to 0.4 (i.e., silicon carbide, water, carbon based materials) and MWs loss insulators for lower $\tan\delta_e$ values (i.e., alumina, polystyrene, polyvinylchloride) [12,44]. The heat dissipation in a MW field is compared to the traditional heating process, Figure 1.

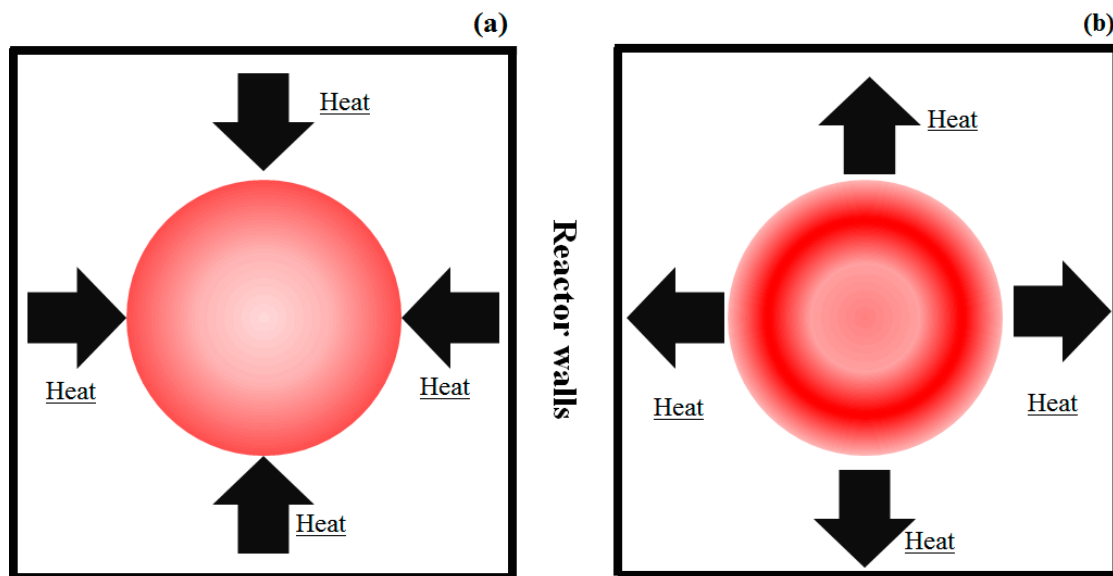


Figure 1. Heat dissipation of same material using (a) traditional heating process and (b) under microwave (MW) field. Deep colour intensity represents higher temperature regions inside the material.

As shown in Figure 1, MW heating is selective and, contrary to traditional heating methodology, avoids the reactor walls effects [45].

The combination of the overall magnetic and electric effects provides the heat-generation rate per unit volume (Q_g) for a generic material:

$$Q_g = \pi f \varepsilon'_o \varepsilon''_r |E|^2 + \pi f \mu'_o \mu''_r |H|^2 \quad (8)$$

According to Bhattacharya et al. [34], Equation (8) could be used to predict the heating rate (HR) of the material as follows:

$$HR = Q_g/\rho_t c_p \quad (9)$$

where ρ_t and c_p are respectively the thermal conductivity and specific heat of the material. Considering Equations (8) and (9), HR is clearly related to both dielectric and magnetic losses of the material. Moreover, HR is affected by several other factors such as the sample size, applied power and reactor configuration. These three parameters induce additional thermal gradients promoting an inhomogeneous heating process.

During MW irradiation, both E and H undergo attenuation phenomena within the material, resulting in a maximum penetration deep (d_p) according to Equation (10):

$$d_p = c(\pi f(2\mu'_r \varepsilon'_r)^{-1/2}((1 + (\varepsilon''_r/\varepsilon'_r)^2(\mu''_r/\mu'_r)^2 + (\varepsilon''_r/\varepsilon'_r)^2 + (\mu''_r/\mu'_r)^2)^{1/2} - (1 - ((\varepsilon''_r \mu''_r)/(\mu'_r \varepsilon'_r))^{-1/2}))^{-1/2} \quad (10)$$

All MW-based processes ranging from telecommunications [46] to chemical conversions (i.e., MAP [47], chemical synthesis [48], sintering [49]) must account for attenuation.

Considering different MW absorber sizes, the attenuation is significant for surfaces and particles large enough to promote the formation of temperature gradients [22] but it is not so relevant for small-sized particles [50] as shown in Figure 2.

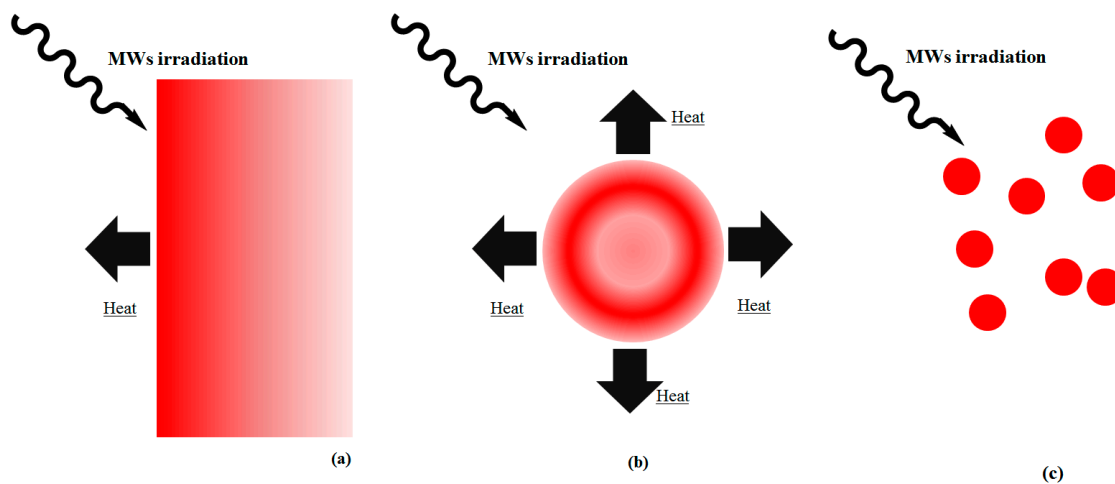


Figure 2. Heat dissipation under MW irradiation considering (a) ideal homogenous, (b) big and (c) small particle-sized MW absorber. Deep colour intensity represents higher temperature regions inside the material.

3. Temperature and Microwave-Assisted Pyrolysis (MAP): Instrumentation and Related Phenomena

3.1. Temperature Measurement Instrumentation

Temperature control is critically important in any pyrolytic treatment [51,52]. Many temperature measurement instruments are currently used for temperature monitoring during pyrolytic processes. As summarized in Table 1, all of them showed some significant drawbacks for direct use during MAP.

Table 1. Summary of common temperature measurement instruments used during pyrolysis with their limitation for microwave assisted pyrolysis (MAP) monitoring.

Temperature Measurement Instrumentation	Behaviour During MAP	Limitations	References
<i>Thermocouple</i>	Able to provide a trustworthy temperature value for reactor walls.	Interactions with MWs. Unable to provide a trustworthy temperature value under direct MWs irradiation.	[53]
<i>Infrared (IR) probe</i>	Able to measure vapour temperature.	Unable to provide a temperature measurement for the feedstock bulk during MAP	[54]
<i>Optical fibers</i>	Able to provide a trustworthy temperature measurement for the feedstock bulk during MAP	Able to provide temperature value of only one spot at the time	[55]

With MWs, standard thermocouples and resistance temperature detectors cannot be used as their metal would interact with the radiation. In 1979, Olsen et al. [56] reported the development of non metal-based thermocouples made with fluorocarbon materials, but suitable only for low temperature uses. Recently, Prathiba et al. [57] described an innovative chromel-alumel thermocouple able to perform measurements in MWs field during the pyrolysis of polystyrene. Also, Liu et al. [58] reported the use of a K-type modified thermocouple used during the study of temperature rise of coal under MWs irradiation. Alternatively, optical fibres could be used [59] but, as reported by Yiping [55], optical fibers undergo perturbative phenomena when they are put into a MW field and require a special calibration and could be trustworthily only for temperature of up to 625 K. Despite this, Gangurte et al. [59] reported how the optical fibre outputs are not significantly able to describe the overall temperature profile of the reactor during the pyrolysis comparing the optical fiber with a thermal camera output for temperatures values of up to 435. However, authors used the optical fibers outputs for calibrate the emissivity in order to produce solid thermal cam outputs.

Some authors reported the use of an infrared thermometer as a reliable tool for temperature measurements [60] but, as illustrated in Figure 3, this approach leads to the measurement of the temperature of pyrolytic vapours, which may differ from the reacting-bed temperature.

Infrared (IR)-based temperature probes accuracy is related to a lot parameters ranging from on the MW wavelength to MW reactor and pyrolytic gas compositions.

This was confirmed by Undri et al. [24] performing MAP of waste tires. Authors reported the use of an IR thermometer to measure the wall and vapour temperatures together with point-by-point measures using optical fibres. These last measurements clearly showed a higher temperature T2 (up to 719 K close to the tires chips) and a lower temperature T1 (close to 617 K) in vapour phase.

Adjusting the emissivity combining an IR probe with an optical fibers is a common practice [61]. Nonetheless, this approach requires a high homogeneity of the feedstock and it is hard to implement for composites materials (i.e., tires, WEEE or beverage packaging). Processing composites involved the unavoidable formation of hotspots that frustrates the IR/optical fibers calibration procedure.

Wang et al. [62] proposed the use of the thermocouple probe directly inserted in the middle of the reactor during the pyrolytic conversion. Notwithstanding this, authors showed the remarkable rise in temperature considering biochar or vapour produced. Similar results were obtained by Mushtaq et al. [63] using two thermocouples placed in different point of the reactor, one on the top and one in the middle of the feedstock. Data collected show increment of temperature gradients up to 474 K after 12 min. Thermocouple approach is generally not trustworthy as reported by Salema et al. [64], mainly because of the slack response, the interference of vapours, the non-uniformity of MWs' intensity and the direct interact with MWs.

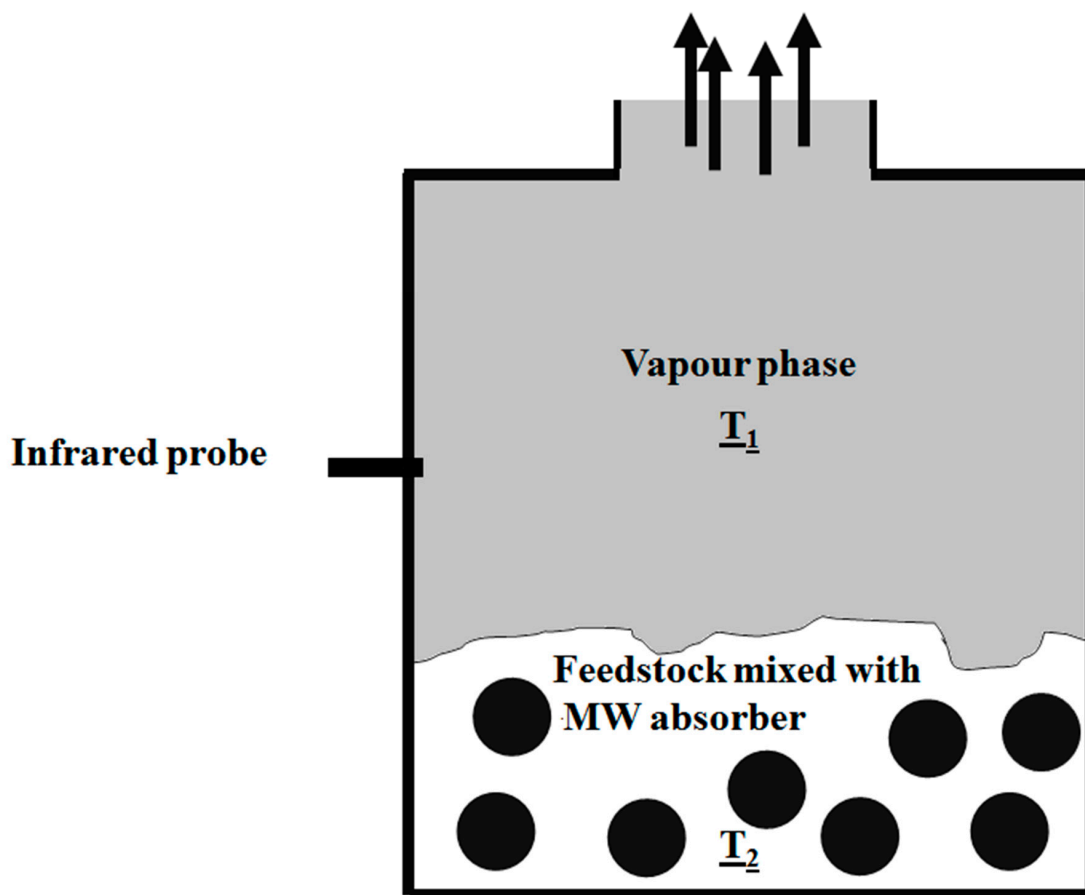


Figure 3. Main problems related to temperature measurements caused by vapour formation during pyrolytic run.

3.2. Feedstock-Induced Variability during MAP

The drop and rise of temperature in a classical pyrolytic unit has been thoroughly studied [65–67]. Motasemi et al. [68] reported a comprehensive computational study of MAP using a computational fluid dynamics model. In that research paper, the authors analyzed simultaneously the relationships among several parameters (i.e., MWs heating, pyrolysis kinetics, phase changes, gas phase transport) and their predictions were in good agreement with experiments reported by Rosi et al. [27] for processing WEEE in a multimode mode batch reactor.

Bartoli et al. [69] established the relationship between MAP products and feedstock particle size for different species of poplar. In this study, using the same process conditions, woody feedstocks with an average diameter below 400 μm sensibly increased the bio-oil fraction. On the contrary, feedstock size up to 3 cm induced gasification. This different behaviour was ascribed to two different phenomena. The first was about the better heat exchange between feedstock and MWs absorbers. The second one was related to thermal inhomogeneity of the feedstock during MAP. During the advancement of the pyrolytic process on the surface of bigger particle, the cracking reaction took place faster than in the particle core. This induced the formation of a carbon layer that increased the MWs' absorption. Despite this, the external particle carbonization induced a pressure increment of the volatile organic compounds released from deep inside the feedstock. This phenomenon is negligible for small particle size, but, in the case of wood chips, it leads to an improvement of radical degradation of the organic matter to small molecules such as water, carbon dioxide and acetic acid. A similar behaviour was reported by Adam et al. [70]. Bartoli et al. [71] also proved that MAP of *Arundo donax* gave different products depending on the part of the plant that was pyrolyzed, e.g., leaves, stems or roots. Klinger et al. [31]

generalized these observations using woody feedstocks, agricultural residues, herbaceous crops and blended feedstocks.

Contrary to common thermal heating processes, heating during MAP can be challenging due to MW–feedstock interactions. Considering MAP, the most commonly processed materials are generally poor MW absorbers (i.e., biomass) or MW insulators (i.e., waste polymers). Consequently, efficient MAP requires the addition of a MWs absorber. The most important observation related to MAP of feedstock mixed with a non-magnetic MW absorber is the close relationship between $\tan\delta_e$ and temperature. As reported by Fan et al. [72], for graphite and graphite-like compounds $\tan\delta_e$ dramatically increased with increasing temperature and similar behaviour could be observed for many materials [73]. The rise in $\tan\delta_e$ leads to unpredictable temperature rising during MAP, resulting in poor temperature control. Uzi et al. [74] studied the permittivity of woody biomass under MAP conditions using an impedance analyzer at different frequencies (from 20 kHz to 3 MHz). They observed a significant increase of $\tan\delta_e$ at 973 K correlating this observation with the increase of aromatic domains formed in the carbon residue during the pyrolytic conversion. A similar behaviour was observed by Allan et al. [75] for cellulose.

Recently, Antunes et al. [76] studied the dielectric properties of biosolids under MW irradiation and demonstrated the necessity of the MWs absorber (i.e., activated carbon, charcoal, biochar, glycerol) even if the feedstock is rich metals [77]. The choice of MWs absorber could also allow gasification temperatures to be reached, as reported by Dong et al. using bamboo as feedstock [78] and an hybrid iron-carbon material as MW absorber. The unpredictable behaviour due to changes in $\tan\delta_e$ could be partially avoided thanks to rapid processing times as reported by several authors [26,79] that lead to completion of MAP conversion fast enough to avoid the major consequences of temperature inhomogeneity. Regarding the homogeneity of the feedstock, several authors [22] reported interesting observations regarding MAP of woody biomass, demonstrating the advantages of using more homogenous wood pellets. Another approach is to complement MAP with exothermic reactions over selected temperature ranges to save energy and achieve a more homogeneous reaction environment, as reported by Wang et al. [62] for corn stover pyrolysis.

Avoiding the classical MAP set-ups, Wang et al. [80] studied a biomass pyrolysis-fluidized bed reactor using MWs merely as heating source for silicon carbide bed. In this case, the volumetric, selective and fast heating process generally associated with MAP was lost but a high control of process temperature was achieved. Contrary to biomasses MAP, MW pyrolytic treatment of plastic materials show a remarkable advantage related to the enhanced interaction with the MW absorber. As a matter of facts, the first stage of plastic MAP is generally the polymer melting with a corresponding improved dispersion of the MW absorbers within the melted feedstock, as shown in Figure 4.

During the pyrolysis of thermoplastic materials (i.e., polystyrene, polyethylene), melting of the polymer occurs first, leading to a well-mixed bulk material inside the reactor as reported by Undri et al. [81,82]. A similar effect could be emulated performing co-pyrolysis under MWs of oil-based cuts mixed with oil sands and biomass [83,84], or with sewage sludge [85]. In these cases, the increased temperature homogeneity could be ascribed to the presence of high boiling point liquids that promote homogenous heat transfer inside the reacting mixture.

The temperature inhomogeneity issue rises again if composite polymers are processed. As shown in Figure 5, different points of the composite material are heated by MW irradiation with different efficiencies. Undri et al. [32] studied the behavior of wasted tires during MAP and used zinc sulfide phase changes to demonstrate the presence hotspots of over 1273 K [29]. Similar behavior could be detected while processing printed board circuits [86,87] and food packaging composites that contain aluminum foil [88]. With such composites, both Q_g and HR are related to the material topology and are deeply affected by metal-containing zones.

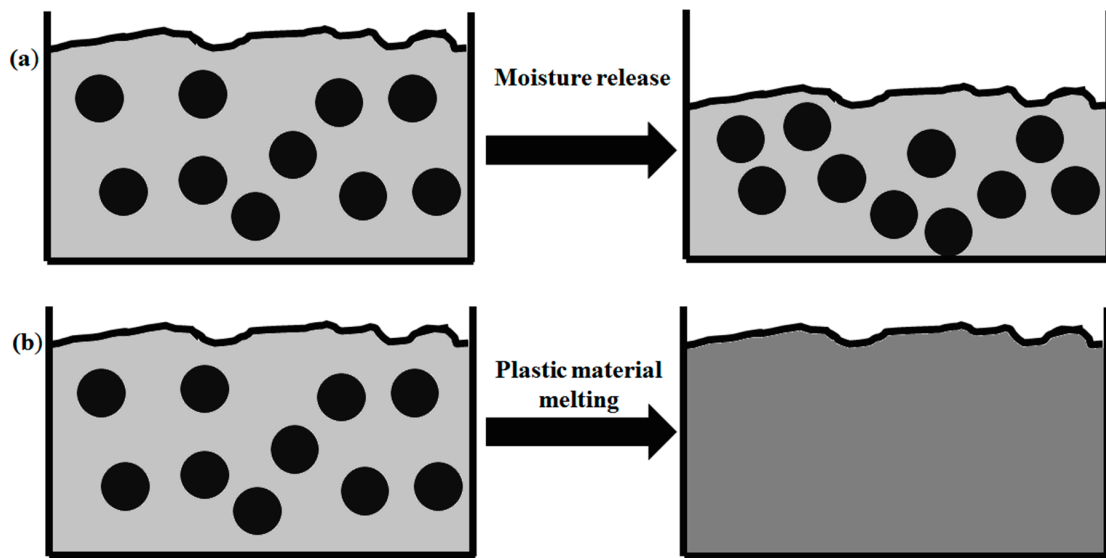


Figure 4. Schematic representation of early stage of (a) biomasses and (b) plastics MAP. Deep colour intensity represents higher temperature regions inside the material.

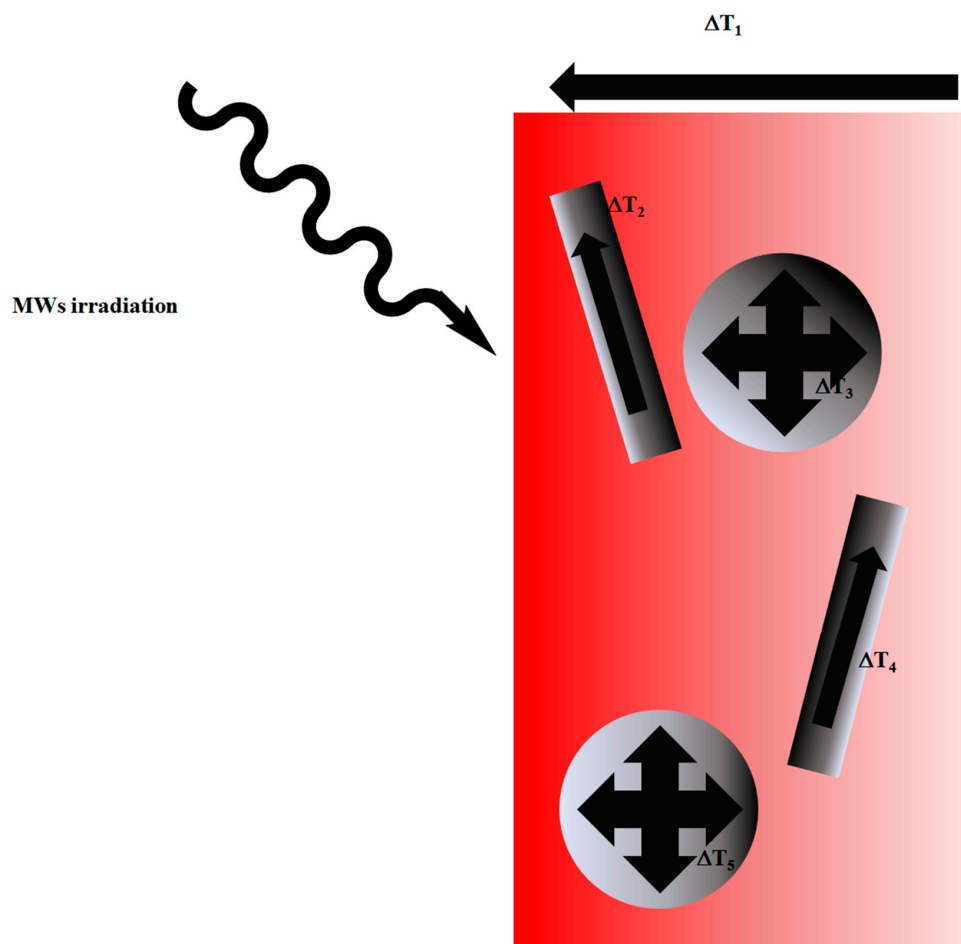


Figure 5. Inhomogeneity heating and multiple temperature gradients (ΔT) inside a composite material with non-homogenous filler shapes. Deep colour intensity represents higher temperature regions inside the material.

Several studies have used the composition of the MAP products to infer the presence of hotspots. Luo et al. [89] showed that during MAP of wood sawdust, phenolic rich bio-oils suggest a bulk temperature of 523–677 K with instantaneous hot spots of around 830 K [90]. Also, Luo et al. [91] showed that with MAP, tar removal over biochar that occurred at a bulk temperature of only 870 K was similar to tar removals observed at temperatures higher than 1000 K in conventional pyrolysis.

As reported above, temperature is not easily controllable during MAP despite its crucial role in the pyrolysis output. Several authors tried to use the ratio of applied power to mass of feedstock as alternative parameter for MAP description [70,92–94]. This approach is quite useful for the realization of a standard process thanks to the relation between MW energy and carbon yields as reported by Budarin et al. [95]. Nonetheless, this approach does not allow for real-time monitoring during MAP and cannot be used for process diagnostics.

3.3. Modelling MW Absorption and Reactors Scale-Up

Simulation methods have helped develop pyrolytic conversions of MAP for plastics [96] and biomasses [97], reported a 3-D mathematical model able to describe resonance phenomena and energy transfer during MWs heating. The numerical predictions were used to develop a prototype with optimized internal patterns of heating altering the phases of the incident waves to achieve a greater uniformity of the final temperature profiles. Models can be used to identify hot and cold spots. Actually, many models have been used to describe MW heating but are generally applied to food science. Nonetheless, they represent a good starting point for complex cases.

Pitchai et al. [98] coupled electromagnetic and heat transfer equations to model complex microwave interactions with food including cavity geometry, phase changes and rotation of the feedstock. Further modeling improvements considered a wide range of wavelengths to improve the accuracy of temperature predictions [99]. Pitchai et al. [100] used a coupled electromagnetic and heat-transfer model to simultaneously optimize several parameters (i.e., cell size, heating time step, and number of iterations for steady state electromagnetic field). The model was validated qualitatively by comparison of predicted and measured temperature profiles, with errors ranging from 0.53 to 4.52 K. Chen et al. [101] showed that decoupling electromagnetics from heat transfer reduces the computational time by up to 90% while achieving similar accuracies in predicted temperatures.

For MAP, Salema et al. [102] reported the results of a numerical simulation of biomass pellets under MW irradiation in a multimode reactor at 2.45 GHz. They were able to predict the location of hot spots that matched the hotspots determined with an experiment. This study led to a scaled-up process for wood pellets MAP [30].

A coupled electromagnetic and heat transfer model was used by Lin et al. [103] to model the MAP of coal at 2.45 GHz. This showed that MW power contributes to the thermal heterogeneity and energy consumption during processes of carbon-based materials. This suggests that low power was suitable for uniform heating and energy saving, while high power applies to differential and rapid heating contrary to what observed for proper pyrolysis processes.

A strong approach was used by Adam et al. [70] simulating volumetric distribution of the electric field inside the reactor cavity. This approach based on Comsol Multiphysics® allowed for the optimization of all reactor parameters from size to waveguides.

4. Conclusions

MAP is a powerful tool for sustainable waste conversion. Despite issues due to the heterogeneity of MW–materials interactions, temperature could be profiled during MAP with both models and direct measurements. The composition of the bio-oil product and the physiochemical characteristics of biochar can also be used to evaluate the range of temperatures reached during MAP treatments. However, a complete trustworthy temperature measurement approach is not available. All the methodologies proposed and described in literature are affected by issues correlated to their interaction with applied MWs and with the inhomogeneity of the feedstock heating. Theoretical calculation could be a helpful

tool for the conceptualization and scalability of MAP processes. The application of such methods will help optimize MAP processes and promote their application to the efficient conversion of biomass and polymer residues.

Considering all this, MAP remains a challenging field that still has great potential for further development.

The optimization of MAP processes should be performed in such a way as to control the reaction temperature. From an engineering process point of view, this is impossible due to the intrinsic heterogeneity of the microwave heating; the only possibility is to measure the local temperatures that could not even represent the average bulk temperature.

MAP engineering processes should be focused on inducing a relatively homogeneous power density distribution through the bulk material in a continuous process setup, since the temperature will be constantly changing due to the highly variable dielectric properties.

Author Contributions: Conceptualization, L.R.; writing—original draft preparation, M.B.; writing—review and editing, L.R., F.B., C.B., M.F.; supervision, L.R., F.B.

Acknowledgments: L.R. wishes to thank The Fondazione Cassa di Risparmio di Firenze (project: “Value from Waste” n. 2014. 0703) for the financial support required to perform this research.

Conflicts of Interest: The authors declare no conflict of interest.

References

- Mohan, S.V.; Nikhil, G.; Chiranjeevi, P.; Reddy, C.N.; Rohit, M.; Kumar, A.N.; Sarkar, O. Waste biorefinery models towards sustainable circular bioeconomy: Critical review and future perspectives. *Bioresour. Technol.* **2016**, *215*, 2–12. [[CrossRef](#)] [[PubMed](#)]
- Chia, S.R.; Chew, K.W.; Show, P.L.; Yap, Y.J.; Ong, H.C.; Ling, T.C.; Chang, J.S. Analysis of economic and environmental aspects of microalgae biorefinery for biofuels production: A review. *Biotechnol. J.* **2018**, *13*, 1700618. [[CrossRef](#)]
- Branchini, L. Waste-to-Energy. In *Waste-to-Energy*; Springer: Berlin/Heidelberg, Germany, 2015; pp. 19–36.
- Haro, P.; Villanueva Perales, A.L.; Arjona, R.; Ollero, P. Thermochemical biorefineries with multiproduction using a platform chemical. *Biofuels Bioprod. Biorefin.* **2014**, *8*, 155–170. [[CrossRef](#)]
- Cantrell, K.B.; Ducey, T.; Ro, K.S.; Hunt, P.G. Livestock waste-to-bioenergy generation opportunities. *Bioresour. Technol.* **2008**, *99*, 7941–7953. [[CrossRef](#)] [[PubMed](#)]
- Mohan, D.; Pittman, C.U.; Steele, P.H. Pyrolysis of wood/biomass for bio-oil: A critical review. *Energy Fuels* **2006**, *20*, 848–889. [[CrossRef](#)]
- Sharuddin, S.; Abnisa, F.; Daud, W.; Aroua, M. Pyrolysis of plastic waste for liquid fuel production as prospective energy resource. *IOP Conf. Ser. Mater. Sci. Eng.* **2018**, *334*, 012001. [[CrossRef](#)]
- Quek, A.; Balasubramanian, R. Liquefaction of waste tires by pyrolysis for oil and chemicals—A review. *J. Anal. Appl. Pyrolysis* **2013**, *101*, 1–16. [[CrossRef](#)]
- Paz-Ferreiro, J.; Nieto, A.; Méndez, A.; Askeland, M.P.J.; Gascó, G. Biochar from Biosolids Pyrolysis: A Review. *Int. J. Environ. Res. Public Health* **2018**, *15*, 956. [[CrossRef](#)]
- Vijayaraghavan, K. A review on biochar feedstocks, production, characterization, modification and potential applications. *J. Environ. Biotechnol. Res.* **2018**, *7*, 11.
- Tian, Y.; Zuo, W.; Ren, Z.; Chen, D. Estimation of a novel method to produce bio-oil from sewage sludge by microwave pyrolysis with the consideration of efficiency and safety. *Bioresour. Technol.* **2011**, *102*, 2053–2061. [[CrossRef](#)]
- Appleton, T.; Colder, R.; Kingman, S.; Lowndes, I.; Read, A. Microwave technology for energy-efficient processing of waste. *Appl. Energy* **2005**, *81*, 85–113. [[CrossRef](#)]
- Lam, S.S.; Chase, H.A. A review on waste to energy processes using microwave pyrolysis. *Energies* **2012**, *5*, 4209–4232. [[CrossRef](#)]
- Ren, S.; Lei, H.; Wang, L.; Bu, Q.; Wei, Y.; Liang, J.; Liu, Y.; Julson, J.; Chen, S.; Wu, J. Microwave torrefaction of Douglas fir sawdust pellets. *Energy Fuels* **2012**, *26*, 5936–5943. [[CrossRef](#)]
- Basu, P. *Biomass Gasification, Pyrolysis and Torrefaction: Practical Design and Theory*; Academic Press: London, UK, 2018.

16. Pyrowave. A Solution to the Global Issue of Plastics End-of-Life Management. Available online: <https://www.pyrowave.com/en/pyrowave-technology> (accessed on 28 August 2019).
17. Robinson, J.; Kingman, S.; Barranco, R.; Snape, C.; Al-Sayegh, H. Microwave pyrolysis of wood pellets. *Ind. Eng. Chem. Res.* **2009**, *49*, 459–463. [[CrossRef](#)]
18. El Khaled, D.; Novas, N.; Gazquez, J.A.; Manzano-Agugliaro, F. Microwave dielectric heating: Applications on metals processing. *Renew. Sustain. Energy Rev.* **2018**, *82*, 2880–2892. [[CrossRef](#)]
19. Mirzaei, A.; Neri, G. Microwave-assisted synthesis of metal oxide nanostructures for gas sensing application: A review. *Sens. Actuators B Chem.* **2016**, *237*, 749–775. [[CrossRef](#)]
20. Green, M.; Liu, Z.; Smedley, R.; Nawaz, H.; Li, X.; Huang, F.; Chen, X. Graphitic carbon nitride nanosheets for microwave absorption. *Mater. Today Phys.* **2018**, *5*, 78–86. [[CrossRef](#)]
21. Zhan, M.; Pan, G.; Wang, Y.; Kuang, T.; Zhou, F. Ultrafast carbon nanotube growth by microwave irradiation. *Diam. Relat. Mater.* **2017**, *77*, 65–71. [[CrossRef](#)]
22. Undri, A.; Zaid, M.; Briens, C.; Berruti, F.; Rosi, L.; Bartoli, M.; Frediani, M.; Frediani, P. Bio-oil from pyrolysis of wood pellets using a microwave multimode oven and different microwave absorbers. *Fuel* **2015**, *153*, 464–482. [[CrossRef](#)]
23. Undri, A.; Rosi, L.; Frediani, M.; Frediani, P. *Microwave Pyrolysis of Polymeric Materials*; Intechopen: London, UK, 2011; 17015.
24. Undri, A.; Meini, S.; Rosi, L.; Frediani, M.; Frediani, P. Microwave pyrolysis of polymeric materials: Waste tires treatment and characterization of the value-added products. *J. Anal. Appl. Pyrolysis* **2013**, *103*, 149–158. [[CrossRef](#)]
25. Işıldar, A.; Rene, E.R.; van Hullebusch, E.D.; Lens, P.N. Electronic waste as a secondary source of critical metals: Management and recovery technologies. *Resour. Conserv. Recycl.* **2018**, *135*, 296–312. [[CrossRef](#)]
26. Bartoli, M.; Rosi, L.; Giovannelli, A.; Frediani, P.; Passaponti, M.; Frediani, M. Microwave assisted pyrolysis of crop residues from *Vitis vinifera*. *J. Anal. Appl. Pyrolysis* **2018**, *130*, 305–313. [[CrossRef](#)]
27. Rosi, L.; Bartoli, M.; Frediani, M. Microwave assisted pyrolysis of halogenated plastics recovered from waste computers. *Waste Manag.* **2018**, *73*, 511–522. [[CrossRef](#)] [[PubMed](#)]
28. Undri, A.; Rosi, L.; Frediani, M.; Frediani, P. Conversion of poly (lactic acid) to lactide via microwave assisted pyrolysis. *J. Anal. Appl. Pyrolysis* **2014**, *110*, 55–65. [[CrossRef](#)]
29. Undri, A.; Sacchi, B.; Cantisani, E.; Toccafondi, N.; Rosi, L.; Frediani, M.; Frediani, P. Carbon from microwave assisted pyrolysis of waste tires. *J. Anal. Appl. Pyrolysis* **2013**, *104*, 396–404. [[CrossRef](#)]
30. Nhuchhen, D.R.; Afzal, M.T.; Dreise, T.; Salema, A.A. Characteristics of biochar and bio-oil produced from wood pellets pyrolysis using a bench scale fixed bed, microwave reactor. *Biomass Bioenergy* **2018**, *119*, 293–303. [[CrossRef](#)]
31. Klinger, J.L.; Westover, T.L.; Emerson, R.M.; Williams, C.L.; Hernandez, S.; Monson, G.D.; Ryan, J.C. Effect of biomass type, heating rate, and sample size on microwave-enhanced fast pyrolysis product yields and qualities. *Appl. Energy* **2018**, *228*, 535–545. [[CrossRef](#)]
32. Undri, A.; Rosi, L.; Frediani, M.; Frediani, P. Upgraded fuel from microwave assisted pyrolysis of waste tire. *Fuel* **2014**, *115*, 600–608. [[CrossRef](#)]
33. Pozar, D.M. *Microwave Engineering*; John Wiley & Sons: Hoboken, NJ, USA, 2009.
34. Bhattacharya, M.; Basak, T. A review on the susceptor assisted microwave processing of materials. *Energy* **2016**, *97*, 306–338. [[CrossRef](#)]
35. Mishra, R.R.; Sharma, A.K. Microwave–material interaction phenomena: Heating mechanisms, challenges and opportunities in material processing. *Compos. Part A Appl. Sci. Manuf.* **2016**, *81*, 78–97. [[CrossRef](#)]
36. Rosenkranz, P.W. Water vapor microwave continuum absorption: A comparison of measurements and models. *Radio Sci.* **1998**, *33*, 919–928. [[CrossRef](#)]
37. Guo, X.; Deng, Y.; Gu, D.; Che, R.; Zhao, D. Synthesis and microwave absorption of uniform hematite nanoparticles and their core-shell mesoporous silica nanocomposites. *J. Mater. Chem.* **2009**, *19*, 6706–6712. [[CrossRef](#)]
38. Clark, D.E.; Folz, D.C.; West, J.K. Processing materials with microwave energy. *Mater. Sci. Eng. A* **2000**, *287*, 153–158. [[CrossRef](#)]
39. Wu, R.; Zhou, K.; Yang, Z.; Qian, X.; Wei, J.; Liu, L.; Huang, Y.; Kong, L.; Wang, L. Molten-salt-mediated synthesis of SiC nanowires for microwave absorption applications. *CrystEngComm* **2013**, *15*, 570–576. [[CrossRef](#)]

40. Ni, Z.; Masel, R.I. Rapid production of metal–organic frameworks via microwave-assisted solvothermal synthesis. *J. Am. Chem. Soc.* **2006**, *128*, 12394–12395. [[CrossRef](#)]
41. Kingman, S.; Rowson, N. Microwave treatment of minerals—A review. *Miner. Eng.* **1998**, *11*, 1081–1087. [[CrossRef](#)]
42. Morgan, S.P., Jr. Effect of surface roughness on eddy current losses at microwave frequencies. *J. Appl. Phys.* **1949**, *20*, 352–362. [[CrossRef](#)]
43. Poole, C.P. *Electron Spin Resonance: A Comprehensive Treatise on Experimental Techniques*; Courier Corporation: New York, NY, USA, 1996.
44. Wong, W.; Gupta, M. *Microwave and Metals*; John Wiley & Sons (Asia): Singapore, 2007.
45. Sazhin, S.S. Modelling of fuel droplet heating and evaporation: Recent results and unsolved problems. *Fuel* **2017**, *196*, 69–101. [[CrossRef](#)]
46. Harden, B.; Norbury, J.; White, W. Use of a lognormal distribution of raindrop sizes in millimetric radio attenuation studies. In *Antennas and Propagation*; International Conference on Antennas and Propagation: London, UK, 1978; pp. 87–91.
47. Farag, S.; Sobhy, A.; Akyel, C.; Doucet, J.; Chaouki, J. Temperature profile prediction within selected materials heated by microwaves at 2.45 GHz. *Appl. Therm. Eng.* **2012**, *36*, 360–369. [[CrossRef](#)]
48. Ahmad, M.; Grössinger, R.; Kriegisch, M.; Kubel, F.; Rana, M. Magnetic and microwave attenuation behavior of Al-substituted Co₂W hexaferrites synthesized by sol-gel autocombustion process. *Curr. Appl. Phys.* **2012**, *12*, 1413–1420. [[CrossRef](#)]
49. Bykov, Y.V.; Rybakov, K.; Semenov, V. High-temperature microwave processing of materials. *J. Phys. D Appl. Phys.* **2001**, *34*, R55. [[CrossRef](#)]
50. Lei, H.; Ren, S.; Julson, J. The effects of reaction temperature and time and particle size of corn stover on microwave pyrolysis. *Energy Fuels* **2009**, *23*, 3254–3261. [[CrossRef](#)]
51. Demirbas, A. Effect of temperature on pyrolysis products from four nut shells. *J. Anal. Appl. Pyrolysis* **2006**, *76*, 285–289. [[CrossRef](#)]
52. Scheirs, J.; Kaminsky, W. *Feedstock Recycling and Pyrolysis of Waste Plastics*; John Wiley & Sons: Chichester, UK, 2006.
53. Dunscombe, P.; McLellan, J.; Malaker, K. Heat production in microwave-irradiated thermocouples. *Med. Phys.* **1986**, *13*, 457–461. [[CrossRef](#)]
54. Budarin, V.L.; Zhao, Y.; Gronnow, M.J.; Shuttleworth, P.S.; Breeden, S.W.; Macquarrie, D.J.; Clark, J.H. Microwave-mediated pyrolysis of macro-algae. *Green Chem.* **2011**, *13*, 2330–2333. [[CrossRef](#)]
55. Yiping, H. Study of microwave field temperature—Measurement error of a fiber optic probe. *Microw. Opt. Technol. Lett.* **1995**, *10*, 62–66. [[CrossRef](#)]
56. Olsen, R.G.; Molina, E.A. The nonmetallic thermocouple: A differential-temperature probe for use in microwave fields. *Radio Sci.* **1979**, *14*, 81–84. [[CrossRef](#)]
57. Prathiba, R.; Shruthi, M.; Miranda, L.R. Pyrolysis of polystyrene waste in the presence of activated carbon in conventional and microwave heating using modified thermocouple. *Waste Manag.* **2018**, *76*, 528–536. [[CrossRef](#)]
58. Liu, H.-P.; Chen, T.-P.; Li, Y.; Song, Z.-Y.; Wang, S.-W.; Wu, S.-H. Temperature rise characteristics of ZhunDong coal during microwave pyrolysis. *Fuel Process. Technol.* **2016**, *148*, 317–323. [[CrossRef](#)]
59. Gangurde, L.S.; Sturm, G.S.; Devadiga, T.J.; Stankiewicz, A.I.; Stefanidis, G.D. Complexity and challenges in noncontact high temperature measurements in microwave-assisted catalytic reactors. *Ind. Eng. Chem. Res.* **2017**, *56*, 13379–13391. [[CrossRef](#)]
60. Morgan, H.M., Jr.; Liang, J.; Chen, K.; Yan, L.; Wang, K.; Mao, H.; Bu, Q. Bio-oil production via catalytic microwave co-pyrolysis of lignin and low density polyethylene using zinc modified lignin-based char as a catalyst. *J. Anal. Appl. Pyrolysis* **2018**, *133*, 107–116. [[CrossRef](#)]
61. Sun, J.; Wang, W.; Liu, Z.; Ma, C. Study of the transference rules for bromine in waste printed circuit boards during microwave-induced pyrolysis. *J. Air Waste Manag. Assoc.* **2011**, *61*, 535–542. [[CrossRef](#)]
62. Wang, X.; Morrison, W.; Du, Z.; Wan, Y.; Lin, X.; Chen, P.; Ruan, R. Biomass temperature profile development and its implications under the microwave-assisted pyrolysis condition. *Appl. Energy* **2012**, *99*, 386–392. [[CrossRef](#)]

63. Mushtaq, F.; Abdullah, T.A.T.; Mat, R.; Ani, F.N. Optimization and characterization of bio-oil produced by microwave assisted pyrolysis of oil palm shell waste biomass with microwave absorber. *Bioresour. Technol.* **2015**, *190*, 442–450. [[CrossRef](#)]
64. Salema, A.A.; Afzal, M.T.; Bennamoun, L. Pyrolysis of corn stalk biomass briquettes in a scaled-up microwave technology. *Bioresour. Technol.* **2017**, *233*, 353–362. [[CrossRef](#)]
65. Kankariya, D.; Briens, C.; Pjontek, D.; Tacchino, S. Effects of liquid feed rate and impeller rotation speed on heat transfer in a mechanically fluidized reactor. *Particuology* **2018**, *39*, 25–32. [[CrossRef](#)]
66. Lago, V.; Greenhalf, C.; Briens, C.; Berruti, F. Mixing and operability characteristics of mechanically fluidized reactors for the pyrolysis of biomass. *Powder Technol.* **2015**, *274*, 205–212. [[CrossRef](#)]
67. Al-Rubeai, J.M.E.; Aliwi, N.M. A Study of Chaotic Behavior of Heat Transfer in Gas-Solid Fluidized Bed. *Eng. Technol. J.* **2010**, *28*, 2027–2042.
68. Motasemi, F.; Gerber, A.G. Multicomponent conjugate heat and mass transfer in biomass materials during microwave pyrolysis for biofuel production. *Fuel* **2018**, *211*, 649–660. [[CrossRef](#)]
69. Bartoli, M.; Rosi, L.; Giovannelli, A.; Frediani, P.; Frediani, M. Bio-oil from residues of short rotation coppice of poplar using a microwave assisted pyrolysis. *J. Anal. Appl. Pyrolysis* **2016**, *119*, 224–232. [[CrossRef](#)]
70. Adam, M.; Beneroso, D.; Katrib, J.; Kingman, S.; Robinson, J.P. Microwave fluidized bed for biomass pyrolysis. Part I: Process design. *Biofuels Bioprod. Biorefin.* **2017**, *11*, 601–612. [[CrossRef](#)]
71. Bartoli, M.; Rosi, L.; Giovannelli, A.; Frediani, P.; Frediani, M. Production of bio-oils and bio-char from *Arundo donax* through microwave assisted pyrolysis in a multimode batch reactor. *J. Anal. Appl. Pyrolysis* **2016**, *122*, 479–489. [[CrossRef](#)]
72. Fan, Y.; Yang, H.; Li, M.; Zou, G. Evaluation of the microwave absorption property of flake graphite. *Mater. Chem. Phys.* **2009**, *115*, 696–698. [[CrossRef](#)]
73. Zhou, D.; Pang, L.-X.; Wang, D.-W.; Qi, Z.-M.; Reaney, I.M. High quality factor, ultralow sintering temperature Li₆B₄O₉ microwave dielectric ceramics with ultralow density for antenna substrates. *ACS Sustain. Chem. Eng.* **2018**, *6*, 11138–11143. [[CrossRef](#)]
74. Uzi, A.; Shen, Y.; Kawi, S.; Levy, A.; Wang, C.-H. Permittivity and chemical characterization of woody biomass during pyrolysis and gasification. *Chem. Eng. J.* **2019**, *355*, 255–268. [[CrossRef](#)]
75. Allan, G.G.; Krieger, B.B.; Work, D.W. Dielectric loss microwave degradation of polymers: Cellulose. *J. Appl. Polym. Sci.* **1980**, *25*, 1839–1859. [[CrossRef](#)]
76. Antunes, E.; Jacob, M.V.; Brodie, G.; Schneider, P.A. Microwave pyrolysis of sewage biosolids: Dielectric properties, microwave susceptor role and its impact on biochar properties. *J. Anal. Appl. Pyrolysis* **2018**, *129*, 93–100. [[CrossRef](#)]
77. Chae, M.; Xia, L.; Zhu, C.; Bressler, D.C. Accelerating settling rates of biosolids lagoons through thermal hydrolysis. *J. Environ. Manag.* **2018**, *220*, 227–232. [[CrossRef](#)]
78. Dong, Q.; Niu, M.; Bi, D.; Liu, W.; Gu, X.; Lu, C. Microwave-assisted catalytic pyrolysis of moso bamboo for high syngas production. *Bioresour. Technol.* **2018**, *256*, 145–151. [[CrossRef](#)]
79. Bartoli, M.; Rosi, L.; Frediani, M.; Undri, A.; Frediani, P. Depolymerization of polystyrene at reduced pressure through a microwave assisted pyrolysis. *J. Anal. Appl. Pyrolysis* **2015**, *113*, 281–287. [[CrossRef](#)]
80. Wang, Y.; Wu, Q.; Duan, D.; Ruan, R.; Liu, Y.; Dai, L.; Zhou, Y.; Zhao, Y.; Zhang, S.; Zeng, Z. Ex-situ catalytic upgrading of vapors from fast microwave-assisted co-pyrolysis of *Chromolaena odorata* and soybean soapstock. *Bioresour. Technol.* **2018**, *261*, 306–312. [[CrossRef](#)]
81. Undri, A.; Frediani, M.; Rosi, L.; Frediani, P. Reverse polymerization of waste polystyrene through microwave assisted pyrolysis. *J. Anal. Appl. Pyrolysis* **2014**, *105*, 35–42. [[CrossRef](#)]
82. Undri, A.; Rosi, L.; Frediani, M.; Frediani, P. Efficient disposal of waste polyolefins through microwave assisted pyrolysis. *Fuel* **2014**, *116*, 662–671. [[CrossRef](#)]
83. Hou, Y.; Qi, S.; You, H.; Huang, Z.; Niu, Q. The study on pyrolysis of oil-based drilling cuttings by microwave and electric heating. *J. Environ. Manag.* **2018**, *228*, 312–318. [[CrossRef](#)]
84. Li, H.; Li, J.; Fan, X.; Li, X.; Gao, X. Insights into the synergetic effect for co-pyrolysis of oil sands and biomass using microwave irradiation. *Fuel* **2019**, *239*, 219–229. [[CrossRef](#)]
85. Lin, K.-H.; Lai, N.; Zeng, J.-Y.; Chiang, H.-L. Temperature influence on product distribution and characteristics of derived residue and oil in wet sludge pyrolysis using microwave heating. *Sci. Total Environ.* **2017**, *584*, 1248–1255. [[CrossRef](#)]

86. Sun, J.; Wang, W.; Liu, Z.; Ma, Q.; Zhao, C.; Ma, C. Kinetic study of the pyrolysis of waste printed circuit boards subject to conventional and microwave heating. *Energies* **2012**, *5*, 3295–3306. [[CrossRef](#)]
87. Sun, J.; Wang, W.; Liu, Z.; Ma, C. Recycling of waste printed circuit boards by microwave-induced pyrolysis and featured mechanical processing. *Ind. Eng. Chem. Res.* **2011**, *50*, 11763–11769.
88. Undri, A.; Rosi, L.; Frediani, M.; Frediani, P. Fuel from microwave assisted pyrolysis of waste multilayer packaging beverage. *Fuel* **2014**, *133*, 7–16. [[CrossRef](#)]
89. Luo, H.; Bao, L.; Kong, L.; Sun, Y. Low temperature microwave-assisted pyrolysis of wood sawdust for phenolic rich compounds: Kinetics and dielectric properties analysis. *Bioresour. Technol.* **2017**, *238*, 109–115. [[CrossRef](#)]
90. Bartoli, M.; Rosi, L.; Giovannelli, A.; Frediani, P.; Frediani, M. Pyrolysis of a-cellulose in a microwave multimode batch reactor. *J. Anal. Appl. Pyrolysis* **2016**, *120*, 284–296. [[CrossRef](#)]
91. Luo, H.; Bao, L.; Wang, H.; Kong, L.; Sun, Y. Microwave-assisted in-situ elimination of primary tars over biochar: Low temperature behaviours and mechanistic insights. *Bioresour. Technol.* **2018**, *267*, 333–340. [[CrossRef](#)]
92. Miura, M.; Kaga, H.; Sakurai, A.; Kakuchi, T.; Takahashi, K. Rapid pyrolysis of wood block by microwave heating. *J. Anal. Appl. Pyrolysis* **2004**, *71*, 187–199. [[CrossRef](#)]
93. Undri, A.; Rosi, L.; Frediani, M.; Frediani, P. Microwave assisted pyrolysis of corn derived plastic bags. *J. Anal. Appl. Pyrolysis* **2014**, *108*, 86–97. [[CrossRef](#)]
94. Adam, M.; Beneroso, D.; Katrib, J.; Kingman, S.; Robinson, J.P. Microwave fluidized bed for biomass pyrolysis. Part II: Effect of process parameters. *Biofuels Bioprod. Biorefin.* **2017**, *11*, 613–624. [[CrossRef](#)]
95. Budarin, V.L.; Shuttleworth, P.S.; Dodson, J.R.; Hunt, A.J.; Lanigan, B.; Marriott, R.; Milkowski, K.J.; Wilson, A.J.; Breeden, S.W.; Fan, J. Use of green chemical technologies in an integrated biorefinery. *Energy Environ. Sci.* **2011**, *4*, 471–479. [[CrossRef](#)]
96. Hujuri, U.; Ghoshal, A.K.; Gumma, S. Modeling pyrolysis kinetics of plastic mixtures. *Polym. Degrad. Stab.* **2008**, *93*, 1832–1837. [[CrossRef](#)]
97. Shen, D.; Fang, M.; Luo, Z.; Cen, K. Modeling pyrolysis of wet wood under external heat flux. *Fire Saf. J.* **2007**, *42*, 210–217. [[CrossRef](#)]
98. Pitchai, K.; Chen, J.; Birla, S.; Gonzalez, R.; Jones, D.; Subbiah, J. A microwave heat transfer model for a rotating multi-component meal in a domestic oven: Development and validation. *J. Food Eng.* **2014**, *128*, 60–71. [[CrossRef](#)]
99. Pitchai, K.; Chen, J.; Birla, S.; Jones, D.; Subbiah, J. Modeling microwave heating of frozen mashed potato in a domestic oven incorporating electromagnetic frequency spectrum. *J. Food Eng.* **2016**, *173*, 124–131. [[CrossRef](#)]
100. Pitchai, K.; Birla, S.L.; Subbiah, J.; Jones, D.; Thippareddi, H. Coupled electromagnetic and heat transfer model for microwave heating in domestic ovens. *J. Food Eng.* **2012**, *112*, 100–111. [[CrossRef](#)]
101. Chen, J.; Pitchai, K.; Jones, D.; Subbiah, J. Effect of decoupling electromagnetics from heat transfer analysis on prediction accuracy and computation time in modeling microwave heating of frozen and fresh mashed potato. *J. Food Eng.* **2015**, *144*, 45–57. [[CrossRef](#)]
102. Salema, A.A.; Afzal, M.T. Numerical simulation of heating behaviour in biomass bed and pellets under multimode microwave system. *Int. J. Therm. Sci.* **2015**, *91*, 12–24. [[CrossRef](#)]
103. Lin, B.; Li, H.; Chen, Z.; Zheng, C.; Hong, Y.; Wang, Z. Sensitivity analysis on the microwave heating of coal: A coupled electromagnetic and heat transfer model. *Appl. Therm. Eng.* **2017**, *126*, 949–962. [[CrossRef](#)]

